2022

Extraction as a Way to Improve the Performance of Microchannel Condensers Using R134a

Jun Li

Pega Hrnjak

Extraction as a way to improve the performance of microchannel condensers using R134a

Jun Li[1,2], Pega Hrnjak[1,3]*

[1]ACRC, the University of Illinois, Urbana, Illinois, USA
pega@illinois.edu

[2]Department of Materials Science and Engineering, University of Michigan, Ann Arbor, Michigan, USA
junlijl@umich.edu

[3]Creative Thermal Solutions, Inc., Urbana, Illinois, USA

* Corresponding Author

ABSTRACT

The present study introduces the concept of extracting liquid refrigerant in microchannel condensers and its potential to enhance condenser performance. The benefit comes at no cost – the condenser geometry is the same except for one or a few well-sized drainage holes in the header baffle. A 1-D finite-volume model is built for the condenser and is validated with R134a experimental data. The capacities agree within ± 5% and the pressure drops agree within ± 35%. Using this model, the performances of a conventional condenser tested in experiments and its extraction counterpart are compared. When the inlet mass flow rate is the same, the extraction condenser lowers the refrigerant outlet temperature by 2.2 K (equivalent to increasing the capacity by 1.6%). When the outlet temperature is the same, the extraction condenser increases the mass flow rate by 2.3%. The reason for the improvement is analyzed thoroughly in terms of the local heat transfer coefficient, refrigerant pressure, refrigerant temperature, and heat transfer rate. The main reason for the higher capacity is attributed to the reduced pressure drop by extraction and thus the higher refrigerant temperature.

1. INTRODUCTION

In an in-tube condensation process, liquid generated on the wall is an extra thermal resistance that reduces the heat flux. Figure 1(a) shows the heat transfer coefficient (HTC) of R134a at different values of mass flux, G, in a 1 mm-inner-diameter microchannel based on the correlations of Cavallini *et al.* (2006). Figure 1(b) shows the corresponding

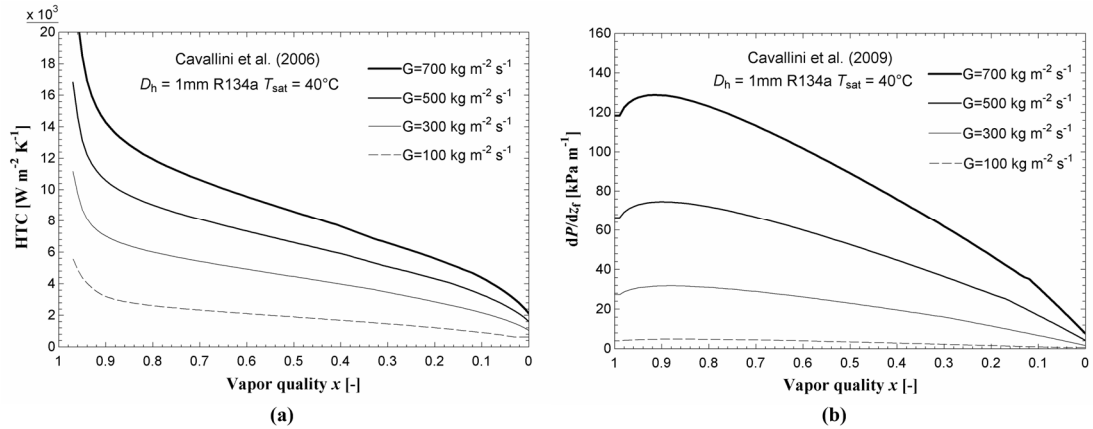

Figure 1: R134a in a 1mm smooth tube at T_{sat} = 40 °C: (a) Heat transfer coefficient (Cavallini et al., 2006); (b) Frictional pressure gradient (Cavallini et al., 2009)

frictional pressure drop gradient $(dP/dz)_f$ based on the correlations of Cavallini *et al.* (2009). When G is a constant, as the vapor quality, x, decreases from around 0.9, representing the formation of liquid condensate, HTC and $(dp/dz)_f$ decrease. The high-x (0.9-1) refrigerant flow can have 5-7 times higher HTC than the low-x (0-0.1) refrigerant flow does. As for the impact of G, at the same x, Figure 1 shows clearly that HTC and $(dp/dz)_f$ become higher as G increases.

Microchannel condensers which are used in mobile and stationary air conditioners usually adopt the multi-pass design. The multi-pass design provides the opportunity to maximize condenser performance by changing G of the refrigerant as condensate is formed, affecting the local HTC and $(dp/dz)_f$. Typically, the number of tubes in each pass decreases as the refrigerant flow proceeds, providing the in-tube HTC_r and pressure (P_r) profiles shown in Figure 2. After a short single-phase zone which represents the superheated vapor flow entering the condenser, HTC_r in Figure 2(a) soon elevates to the maximum where the bulk quality of the refrigerant flow equals 1. Then, based on the trends in Figure 1(a), HTC_r falls as the refrigerant flow proceeds. The discontinuity at the entrance of each pass is because of the increased mass flux. P_r in Figure 2(b) decreases as the refrigerant flow proceeds, which is mainly because the frictional pressure drop dominates the decelerational pressure increase. The decelerational pressure increase is generally a few hundredths of the frictional pressure drop.

2. CONCEPT OF LIQUID EXTRACTION

From Figure 1, in the same flow passage, removing the liquid phase during condensation will increase x and may increase HTC, with the trade-off of reduced G which will decrease HTC. On the other hand, reduced G will decrease $(dp/dz)_f$, with the trade-off by increased x. Just as shown by Figure 1(b), usually the effect of G on $(dp/dz)_f$ is much larger than the effect of x, so the benefit of reduction in pressure drop is almost always ensured. Therefore, removing liquid during condensation can be a way to improve the performance of a condenser.

In a multi-pass microchannel condenser, an intermediate header can be a perfect location to remove liquid, and the cost may not be high. Two inexpensive pass circuitries can realize this goal: the separation circuitry and the extraction circuitry. The separation circuitry refers to separating liquid from vapor and then reassigning the flow passages for the separated vapor flow and liquid flow. Details can be found in Li and Hrnjak (2017a; 2017b; 2021a; 2021b).

The extraction circuitry for microchannel condensers can be designed as shown non-exhaustively in Figure 3, which covers designs for 3-pass to 5-pass condensers. We are only focusing on single-slab, parallel-tube, cross-flow microchannel condensers. Different from the separation circuitry, the extraction circuitry is designed to extract liquid flow in one or several vertical intermediate headers through a well-designed hole in the lower baffle of the header. The liquid flow is directed to the exit of the condenser or the entrance of downstream passes. The liquid flow will move downward through the hole based on the pressure difference.

If the liquid can be drained efficiently, the flow rate in downstream passes will be smaller, thus effectively reducing

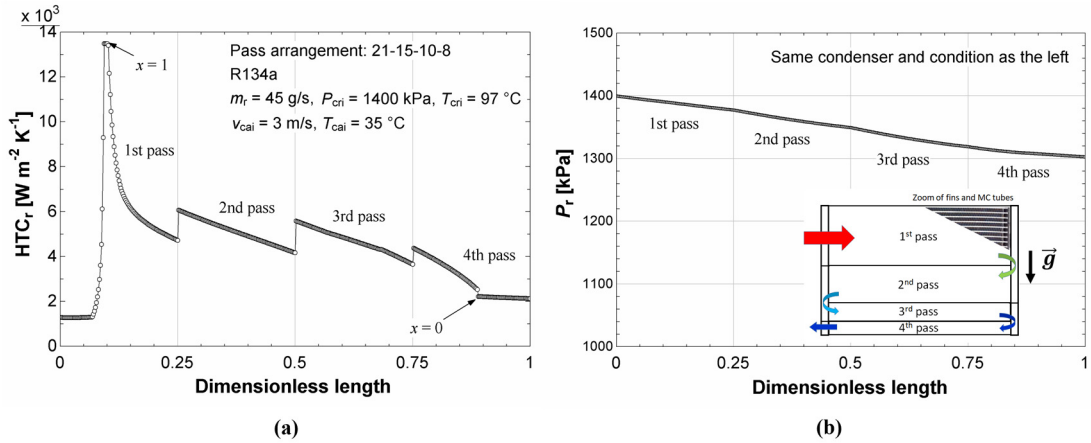

Figure 2: Heat transfer coefficient and pressure in a typical microchannel condenser: (a) heat transfer coefficient; (b) pressure (inset: schematic of the condenser)

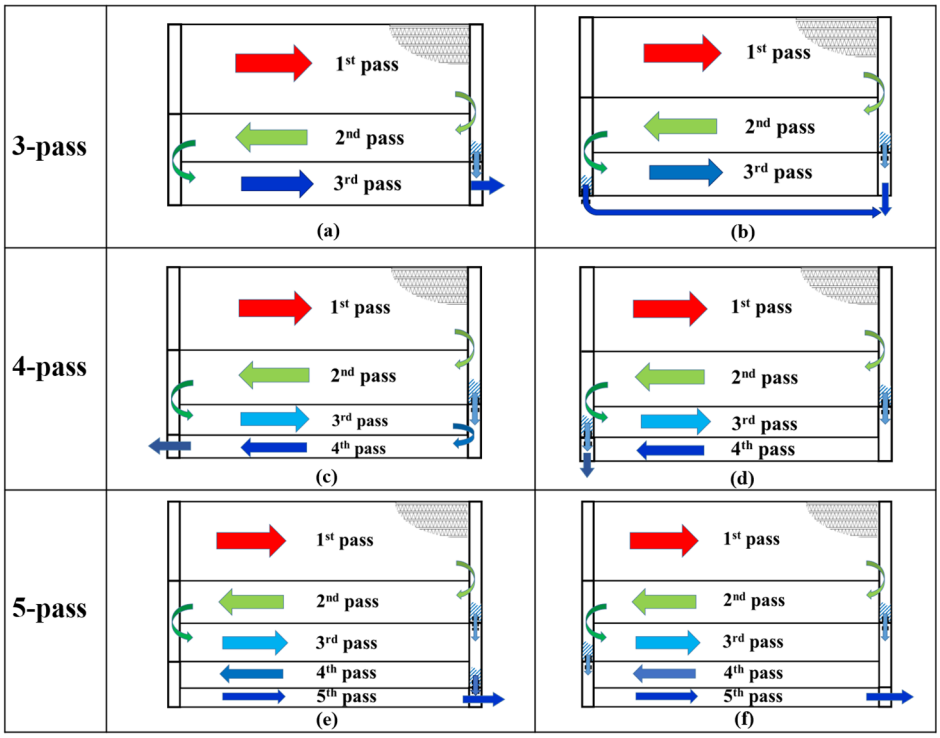

Figure 3: Some possible circuitries for extraction condensers

the pressure drop. Reduced pressure drop increases the saturation temperature of the refrigerant and increases the LMTD of the condenser. From the heat transfer point of view, after the same 1st pass, extraction leaves the flow at the inlet of the downstream pass close to the onset of condensation, where the HTC is the highest. These factors may increase the heat transfer rate, i.e. capacity, of the downstream pass.

Figure 4 shows the nomenclature for quantification of the liquid and vapor extraction in the second header. Two efficiencies are defined for liquid and vapor, respectively. The liquid extraction efficiency, η_L, is defined as the ratio of the liquid mass flow rate through the extraction hole to the total liquid mass flow rate coming into the header, as shown by Eq. (1). The vapor separation efficiency, η_V, is evaluated as the ratio of the vapor mass flow rate going into the downstream pass to the total vapor mass flow rate entering the header, as shown by Eq. (2).

$$\eta_L = \frac{\dot{m}_{L,ex}}{\dot{m}_{L,ex} + \dot{m}_{2Li}} \tag{1}$$

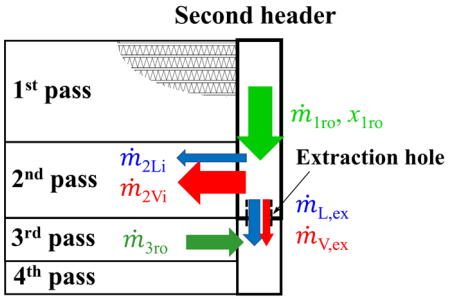

Figure 4: Parameters related to the definition of separation efficiencies of the second header

$$\eta_V = \frac{\dot{m}_{2Vi}}{\dot{m}_{2Vi} + \dot{m}_{V,ex}} \quad (2)$$

where $\dot{m}_{V,ex}$ and $\dot{m}_{L,ex}$ are the vapor mass flow rate and liquid mass flow rate extracted through the extraction hole; $\dot{m}_{2Vi}$ and $\dot{m}_{2Li}$ are the vapor mass flow rate and liquid mass flow rate at the inlet of the 2nd pass.

The ranges for both η_L and η_V are [0, 1]. In the present study, we assume a complete separation of liquid from vapor in the second header, i.e., $\eta_L = 1$ and $\eta_V = 1$. Real separation efficiency and the size of the orifice hole will be experimentally quantified in our upcoming work.

The objective of the present study is to provide a theoretical basis for the improvement of microchannel condensers by liquid extraction. Using an experimentally validated model, the effect of liquid extraction on the heat transfer of the condenser is studied. In-tube heat transfer and pressure drop characteristics are analyzed.

3. EVALUATION OF THE CONCEPT

The performance of two condensers from a major heat exchanger manufacturer is evaluated and compared by a condenser model. We use two methods for the comparison. The two condensers are also evaluated by experiments, which will be presented in a separate study. The experimental results are used to validate the model in this study.

3.1 Model description

Park and Hrnjak (2008) built a steady-state microchannel condenser model using the 1-D finite-volume discretization. We adopt the same methodology to model our microchannel condenser under state-state operation with and without liquid extraction.

The following assumptions are made for one pass of the condenser: (1) refrigerant flow distribution is uniform among the microchannel tubes; (2) refrigerant flow distribution is uniform among the microchannel ports in one microchannel tube; (3) no heat is conducted along the tube nor between tubes through fins; (4) all headers are adiabatic; (5) the pressure drop in headers is neglected; (6) incoming air has a uniform temperature and velocity profile.

The empirical correlations for heat transfer and pressure drop are listed in Table 1. The heat transfer correlation for the condensing superheated region and the condensing subcooled region is referred to (Xiao and Hrnjak, 2017). The refrigerant properties are calculated by REFPROP 10.0 (Lemmon et al., 2018). The simulation is carried out in MATLAB 2018a.

Table 1: Summary of heat transfer and pressure drop correlations

Item	**Correlation**
Air side	
Heat transfer coefficient	Chang and Wang (1997)
Pressure drop	Chang and Wang (1996)
Refrigerant side – Single-phase region	
Heat transfer coefficient	Gnielinski (1976)
Frictional pressure drop	Churchill (1977)
Refrigerant side – Two-phase region	
Heat transfer coefficient	Cavallini *et al.* (2006)
Frictional pressure drop	Cavallini *et al.* (2006)
Deceleration pressure drop	Cavallini *et al.* (2009)
Refrigerant side – Condensing superheated region and condensing subcooled region	
Heat transfer coefficient	Xiao and Hrnjak (2017)

3.2 Experimental validation of the model

A single-slab, 4-pass, cross-flow microchannel condenser from a major heat exchanger manufacturer for vehicular air conditioners is selected to validate the condenser model. Figure 5 shows the pass circuity schematic of this condenser and names it the conventional condenser. Figure 5 also includes its corresponding extraction design for performance comparison and names it the extraction condenser. The number of microchannel tubes is marked for each pass. The extraction design falls into the category represented by Figure 3(c): liquid is extracted at the bottom of the second header and sent to the inlet to the 4th pass.

Table 2 presents the main geometrical dimensions of the condenser. One microchannel port in one microchannel tube has a hydraulic diameter of 0.67 mm. The number of microchannel ports per tube is 16. The fin density of the condenser is 17 per inch, the face area 0.2447 m^2, the total air-side area 5.2895 m^2, and the total refrigerant-side area 1.3232 m^2.

Experiments for the conventional condenser in Figure 5 are conducted on a mobile air conditioning test facility. It can be referred to in Li and Hrnjak (2017a). The working fluid is R134a. The compressor uses PAG 46 synthetic oil. 81 data points are obtained under operating conditions per SAE Standard J2765 (SAE International, 2008). The air inlet temperature is set to be 35 ºC, 40 ºC, or 45 ºC. The air face velocity is in the range of 1.6 – 3.7 m/s. The R134a-oil mixture outlet pressure (P_{cmo}) used to calculate the saturation temperature for the condenser ranges from 860.4 to 1827.5 kPa. The R134a-oil mixture mass flow rate ($\dot{m}_m$) ranges from 24.5 to 46.0 g/s, which corresponds to mass flux through the 1st pass of 197 – 368 kg/(m^2-s). The subcooling (i.e., the difference between the saturation temperature and the temperature) at the condenser outlet is controlled in the range of 0 – 22.6 K.

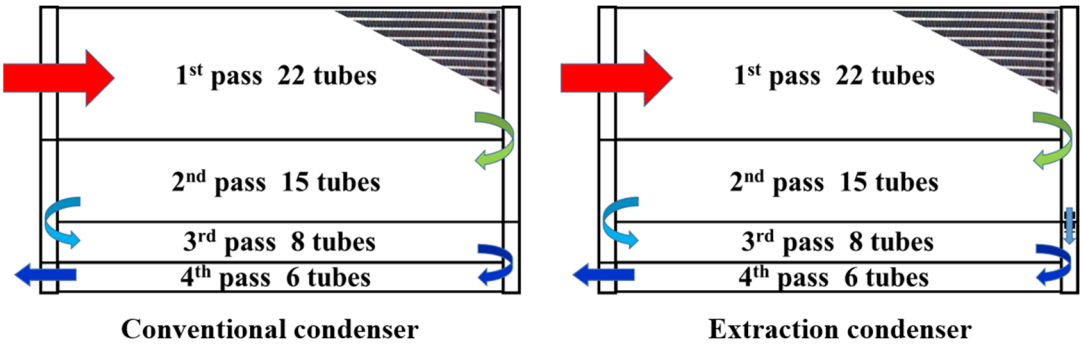

Figure 5: Schematics of the 4-pass conventional microchannel condenser and its corresponding extraction design

Table 2: Main geometrical dimensions of the microchannel condenser in Figure 5

Item	Value	Item	Value
Width w. headers [mm]	620	Louver pitch [mm]	0.77
Width w/o headers [mm]	590	Louver length [mm]	6.0
Width covered by fin [mm]	575	Louver angle [-]	27
Height w/ side plates [mm]	405	Header type	D-shape
Height w/o side plates [mm]	390	Header equivalent diameter [mm]	18.0
Depth [mm]	16.0	Length of the extraction tube [mm]	2200
MC tube thickness [mm]	1.0	Diameter of the extraction tube [mm]	3.175
MC tube pitch [mm]	7.8	Length of the vapor extraction tube [mm]	2400
MC port D_h [mm]	0.67	Diameter of the vapor extraction tube [mm]	6.35
Number of MC ports per tube [-]	16	Length of the liquid extraction tube [mm]	2550
Fin thickness [mm]	0.1	Diameter of the liquid extraction tube [mm]	3.175
Fin pitch [mm]	1.53		

Figure 6 shows the comparison between the experimental results and the modeling results for the heating capacity Q_c and the pressure drop ΔP_c of the condenser. Figure 6(a) shows the comparison of predicted and measured Q_c. 98% of the data points are predicted within +/-5% deviation from the experimental results. Figure 6(b) compares the predicted and measured ΔP_c. 88% of the data points are predicted within ±35% deviation from the experimental results. Overall, the modeling results show good agreement with the experimental results.

Not only the pressure drop in the whole condenser is measured, but the pressure drop in the 1st pass (ΔP_1) and the first three passes ($\Delta P_{1\text{-}3}$) are also measured. Figure 7(a) shows the comparison between the experimental results and the modeling results for ΔP_1. Figure 7(b) shows the comparison for $\Delta P_{1\text{-}3}$. Only 58% of the data points are predicted within ±35% deviation from the experimental results in Figure 7(a), and 80% of the data points are underpredicted. Meanwhile, all data points are predicted within ±35% deviation from the experimental results in Figure 7(b). The

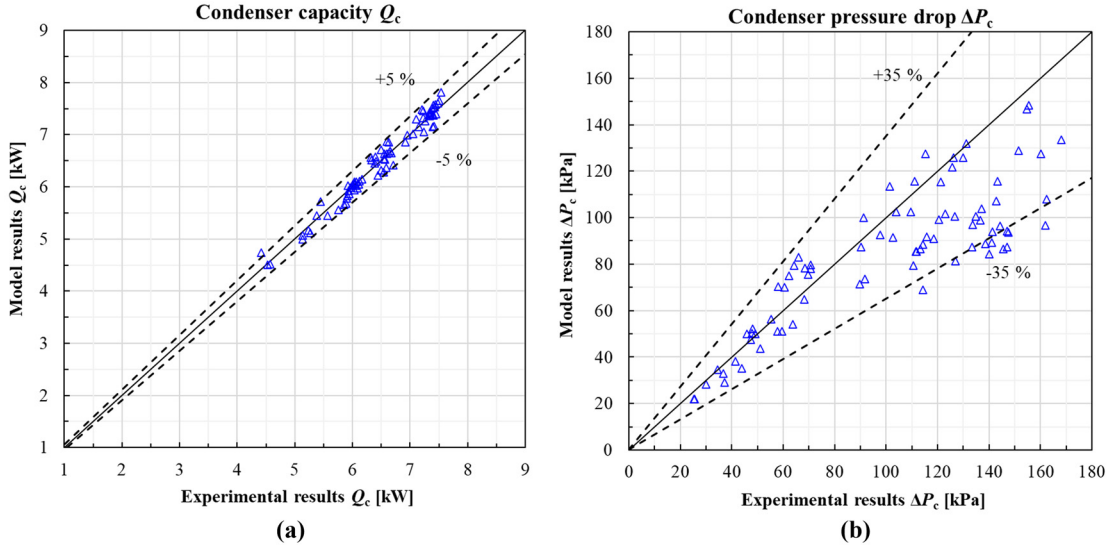

Figure 6: Comparison of the experiment results and the model results: (a) condenser capacity; (b) condenser pressure drop

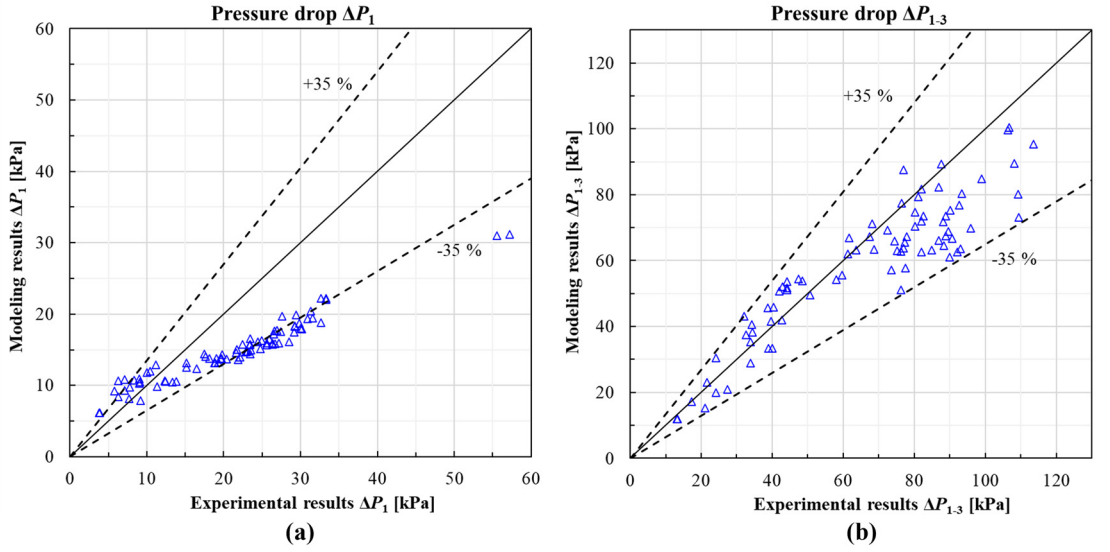

Figure 7: Comparison of the experiment results and the model results: (a) refrigerant pressure drop in the 1st pass; (b) refrigerant pressure drop in the 1st pass to the 3rd pass

reason for the underpredicted ΔP_1 is probably because the pressure drop in the header is neglected, as stated in the assumptions for the condenser model. While the pressure drop in header is higher in the 1st pass due to the higher quality of the refrigerant flow, neglecting the pressure drop in header has a bigger impact on ΔP_1 than on $\Delta P_{1\text{-}3}$ or ΔP_c.

3.3 Results

The performance of the two condensers in Figure 5 is compared by using the condenser model. On the refrigerant-oil-mixture side of a condenser, the condenser capacity is calculated as Eq. (3):

$$Q_c = \dot{m}_m \left(h_{cmi} - h_{cmo} \right) \tag{3}$$

where $\dot{m}_m$ is the mass flow rate of the refrigerant-oil mixture, h_{cmi} is the inlet specific enthalpy of the refrigerant-oil mixture, and h_{cmo} is the outlet specific enthalpy of the refrigerant-oil mixture.

We assume oil is fully miscible in liquid refrigerant, and there is no heat of mixing. Refrigerant and oil are also assumed to have a uniform temperature and pressure on one cross-section in the pipeline. The specific enthalpy of the mixture (h_m) at one location of the pipeline of the refrigeration system can be expressed as

$$h_m = \left(1 - \mathrm{OCR}\right) h_r + \mathrm{OCR}\, h_o \tag{4}$$

where h_r is the refrigerant specific enthalpy, h_o is the oil specific enthalpy, and OCR is the oil circulation ratio. h_r and h_o are determined using the same temperature and pressure at that location.

The criteria to compare these two condensers are selected to be the same as those used in (Li and Hrnjak, 2017b) on the heat-exchanger level, and they are shown in Table 3. The air-side inlet conditions for the two condensers are maintained the same. For the exit enthalpy criterion in Table 3, $\dot{m}_m$ and h_{cmi} are maintained the same. Based on Eq. (3), the condenser with a lower h_{cmo} has a higher capacity Q_c, thus it is more effective. For the condensate flow rate criterion in Table 3, h_{cri} and h_{cro} are maintained the same. Based on Eq. (3) again, the condenser with a higher $\dot{m}_m$ has a higher Q_c, thus it is more effective.

For each comparison condition in this study, the condenser has subcooled refrigerant at the outlet to reflect a realistic operating condition. Based on the thermophysical properties of refrigerants, in the superheated state or the subcooled state, the specific enthalpy of a refrigerant is only a function of the temperature. Therefore, a lower condenser outlet temperature (T_{cmo}) means a lower h_{cmo}.

An R134a operating condition is chosen from the experimental data in Figure 6 to compare the extraction condenser and the conventional condenser. All parameters of this operating condition are inlet parameters and listed in Table 4.

Figure 8 shows the extraction condenser outperforms the conventional condenser using the two criteria in Table 3. Using the exit enthalpy criterion, Figure 8(a) shows that the extraction condenser has a lower T_{cmo} (33.5 °C) than the conventional condenser (35.7 °C), so the extraction condenser is more effective than the conventional condenser. As shown in Figure 8(b), the corresponding capacity increase is 1.6%. Using the condensate flow rate criterion, Figure 8(c) shows $\dot{m}_m$ of the extraction condenser is higher than that of the conventional condenser by 2.3%, which is equal to the percental improvement in Q_c as well.

Table 3 Criteria set for the comparison of the two condensers

	Constants		**Parameter to compare**
	Refrigerant side	Air side	
Exit enthalpy criterion	P_{cmi}, T_{cmi}, $\dot{m}_m$, OCR	T_{cai}, RH_{cai}, v_{cai}	h_{cmo} / T_{cmo}
Condensate flow rate criterion	P_{cmi}, T_{cmi}, h_{cmo}, OCR	T_{cai}, RH_{cai}, v_{cai}	$\dot{m}_m$

Table 4 R134a operating condition for the simulation

Parameter	Value
P_{cmi} [kPa]	1075
T_{cmi} [°C]	70
$\dot{m}_m$ [g/s]	43.5
OCR [-]	5%
T_{cai} [°C]	25
RH_{cai} [-]	35%
v_{cai} [m/s]	4.0

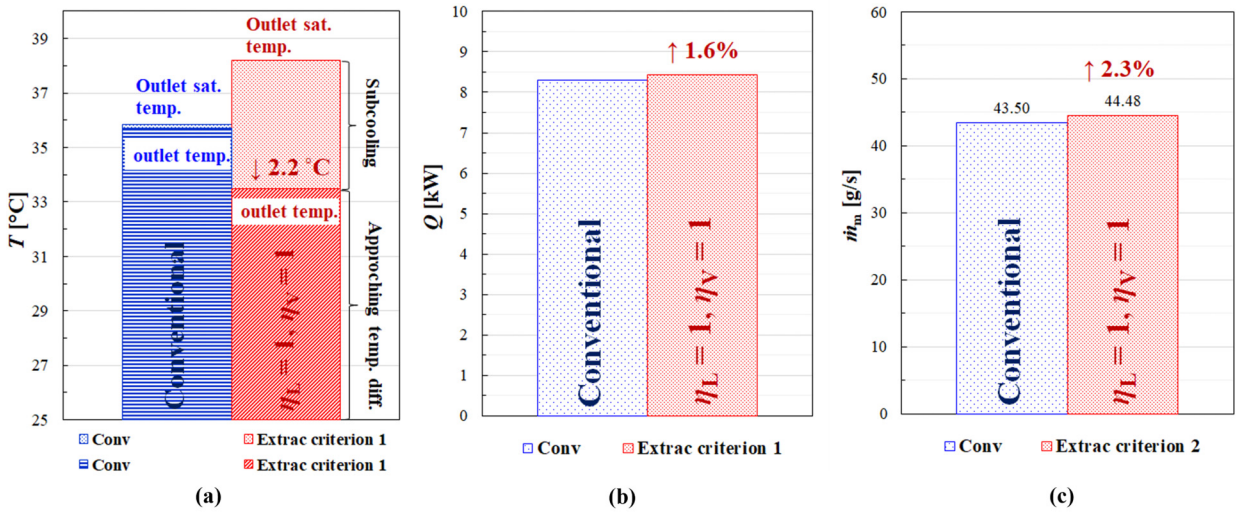

Figure 8: (a) Lower T_{cmo} for the extraction condenser using criterion 1 (condition in Table 4); (b) Higher Q_c for the extraction condenser using criterion 1 (condition in Table 4); (c) Higher $\dot{m}_m$ for the extraction condenser using criterion 2 (P_{cmi} = 1075 kPa, T_{cmi} = 70 °C, T_{cmo} = 35.7 °C, OCR = 5%, T_{cai} = 25 °C, RH_{cai} = 35%, v_{cai} = 4 m/s)

To explain the reason for the improvement in Figure 8(a-b), Figure 9(a-d) show the profiles of HTC_r, U, P_r, and T_r for the extraction condenser and the conventional condenser. $\dot{m}_{2ri}$ = 23.7 g/s after the liquid extraction in the second header. It can be concluded from Figure 9(a) that although $HTC_{r,ex}$ has a spike at the inlet of the 2nd pass due to high inlet quality, it reduces quickly. Plus, due to lower mass flux than the conventional, $HTC_{r,ex}$ actually becomes lower than $HTC_{r,conv}$ as the flow proceeds to the downstream 3/4 length of the 2nd pass. It is clear that $HTC_{r,ex}$ is also lower than $HTC_{r,conv}$ for all flow passages of the 3rd pass and the 4th pass. With a constant HTC_a, U shares the same trend as HTC_r, as shown in Figure 9(b). It is worth noting that because U takes into account a much lower constant HTC_a, the relative improvement in U for the extraction condenser decreases compared to the improvement in HTC_r. Figure 9(a-b) demonstrate that the improvement by extraction on heat transfer is not drastic and exists for a short length after liquid extraction.

Nevertheless, due to the lower mass flux in the 2nd pass and the 3rd pass compared to the total mass flux, the benefit in pressure drop can be confirmed. Figure 9(c) shows a 61 kPa reduction in ΔP_c for the extraction condenser compared to the conventional baseline. Because $P_{r,ex}$ is higher than $P_{r,conv}$ entering the 2nd pass, so is $T_{r,ex}$ compared to $T_{r,conv}$, as shown in Figure 9(d). This increases the refrigerant-air temperature difference and compensates for the penalty in HTC.

4. SUMMARY AND CONCLUSION

This study presents the concept of liquid extraction in the second header for a microchannel condenser. A 1-D

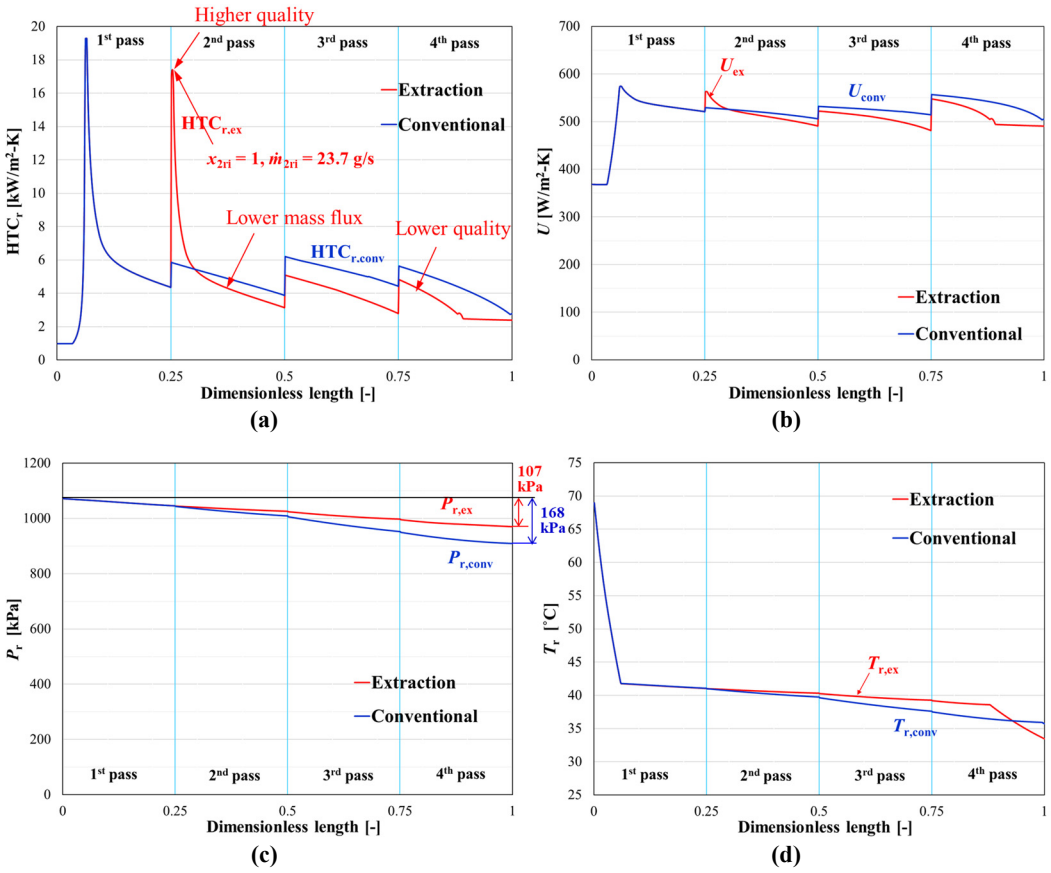

Figure 9: In-tube analysis for the extraction condenser and the conventional condenser (inlet condition in Table 4): (a) refrigerant-side heat transfer coefficient; (b) overall heat transfer coefficient; (c) refrigerant pressure; (d) refrigerant temperature

numerical model is built to predict the performance of the condenser and validated with the experimental data. Most of the data for the capacity agree within ±5 % and most of the data for the pressure drop agree within ± 35%.

Assuming $\eta_L = \eta_V = 1$, the capacity of the extraction condenser is higher than the conventional condenser by 1.6% (refrigerant outlet temperature lower by 2.2 K). The mass flow rate of the extraction condenser is higher than the conventional condenser by 2.3%. Based on detailed in-tube analysis on heat transfer and pressure drop, the main reason for the higher capacity is attributed to the reduced pressure drop by extraction and thus a higher refrigerant temperature.

The experimental confirmation of the improvement and the experimental quantification of the separation efficiency in header have been conducted in another study by the same authors.

NOMENCLATURE

D	diameter	(m)
ΔP	pressure drop	(kPa)
$\dot{m}$	mass flow rate	(g/s)
OCR	oil circulation ratio	(-)
P	pressure / pitch	(kPa) / (mm)
Q	capacity	(kW)
RH	relative humidity	(-)
T	temperature	(°C)
U	overall heat transfer coefficient	(W/m^2-K)

v	velocity	(m/s)
x	vapor quality	(-)

Greeks

η	separation efficiency	(-)
ρ	density	(kg/m^3)

Subscripts

1-3	1st pass to 3rd pass	cri	condenser refrigerant inlet
1ro	1st pass refrigerant outlet	cro	condenser refrigerant outlet
2Li	2nd pass liquid inlet	ex	extraction
2ri	2nd pass refrigerant inlet	f	frictional
2Vi	2nd pass vapor inlet	h	hydraulic
3ro	3rd pass refrigerant outlet	L	liquid
c	condenser	m	refrigerant-oil mixture
cai	condenser air inlet	r	refrigerant
cmi	condenser mixture inlet	sat	saturation
cmo	condenser mixture outlet	V	vapor
conv	conventional		

REFERENCES

Cavallini, A., Doretti, L., Matkovic, M., & Rossetto, L. (2006). Update on Condensation Heat Transfer and Pressure Drop inside Minichannels, *Heat Trans. Eng.*, 27(4), 74-87.

Cavallini, A., Del Col, D., Matkovic, M., & Rossetto, L. (2009). Frictional Pressure Drop During Vapour–Liquid Flow in Minichannels: Modelling and Experimental Evaluation, *Int. J. Heat Fluid Flow*, *30*(1), 131-139.

Chang, Y.J., & Wang, C.C. (1997). A Generalized Heat Transfer Correlation for Louver Fin Geometry, *Int. J. Heat Mass Transfer*, *40*(3), 533-544.

Chang, Y.J., & Wang, C.C. (1996). Air Side Performance of Brazed Aluminum Heat Exchangers, *J. Enhanced Heat Transfer*, *3*(1), 15-28.

Churchill, S.W. (1977). Friction-factor equation spans all fluid-flow regimes, *Chem. Eng.*, 84(24), 91-92.

Gnielinski, V. (1976). New equation of heat and mass transfer in turbulent pipe and channel flow, *Int. Chem. Eng.*, *16*(2), 359-368.

Lemmon, E.W., Bell, I.H., Huber, M.L., & McLinden, M.O. (2018). Reference Fluid Thermodynamic and Transport Properties Database – REFPROP, Version 10.0, U.S. Secretary of Commerce.

Li, J., & Hrnjak, P. (2017a). Improvement of condenser performance by phase separation confirmed experimentally and by modeling. *Int. J. Refrig.*, *78*, 60-69.

Li, J., & Hrnjak, P. (2017b). Separation in condensers as a way to improve efficiency. *Int. J. Refrig.*, *79*, 1-9.

Li, J., & Hrnjak, P. (2021a). An experimentally validated model for microchannel condensers with separation circuitry. *Appl. Therm. Eng.*, *183*, 116114.

Li, J., & Hrnjak, P. (2021b). Optimization of a microchannel condenser with separation circuitry. *Appl. Therm. Eng.*, *184*, 116273.

Park, C.Y., & Hrnjak, P. (2008). Experimental and numerical study on microchannel and round-tube condensers in a R410A residential air-conditioning system. *Int. J. Refrig.*, *31*(5), 822-831.

SAE International. (2008). Procedure for Measuring System COP [Coefficient of Performance] of a Mobile Air Conditioning System on a Test Bench, SAE Surface Vehicle Standard J2765 OCT2008.

Xiao, J., & Hrnjak, P. (2017). A heat transfer model for condensation accounting for non-equilibrium effects. *Int. J. Heat and Mass Transfer*, *111*, 201-210.

ACKNOWLEDGMENT

The research presented in this paper was part of the postdoctoral work of Jun Li, which was funded through the Air Conditioning and Refrigeration Center (ACRC Project #441) at the University of Illinois. The authors would like to thank the financial support from the ACRC and the technical support from Creative Thermal Solutions, Inc.